Electron Transfer Mediated by Surface-Tethered Redox Groups in Nanofluidic Devices

Tom Steentjes, Sahana Sarkar, Pascal Jonkheijm, Serge G. Lemay, and Jurriaan Huskens**

***E**lectrochemistry provides a powerful sensor transduction and amplification mechanism that is highly suited for use in integrated, massively parallelized assays. Here, the cyclic voltammetric detection of flexible, linear poly(ethylene glycol) polymers is demonstrated, which have been functionalized with redox-active ferrocene (Fc) moieties and surface-tethered inside a nanofluidic device consisting of two microscale electrodes separated by a gap of <100 nm. Diffusion of the surface-bound polymer chains in the aqueous electrolyte allows the redox groups to repeatedly shuttle electrons from one electrode to the other, resulting in a greatly amplified steady-state electrical current. Variation of the polymer length provides control over the current, as the activity per Fc moiety appears to depend on the extent to which the polymer layers of the opposing electrodes can interpenetrate each other and thus exchange electrons. These results outline the design rules for sensing devices that are based on changing the polymer length, flexibility, and/or diffusivity by binding an analyte to the polymer chain. Such a nanofluidic enabled configuration provides an amplified and highly sensitive alternative to other electrochemical detection mechanisms.*

1. Introduction

Biosensing plays an increasingly important role, in particular, in the development of personalized medicine.[1] This growing importance also puts new demands on the performance of such devices, which ranges from higher sensitivities and selectivities, to the use of smaller sample volumes, the use of body fluids, an easy readout and signal processing, and the option to use disposable devices. Electrochemical devices have particular advantages that meet several of these requirements.[2] The combination with electrochemistry opens pathways for a multitude of benefits for biosensing strategies that allow their use in personalized medicine.[3] A key opportunity offered by electrochemistry is an enhanced sensitivity based on signal amplification, which can be achieved when multiple electrons, e.g., in cyclic redox processes, amplify a single molecular recognition event.

Prime examples of sensitive electrochemical detection are redox-activated DNA biosensors, which rely on conformational changes that modulate the motion and the distance of the redox moiety to an electrode, resulting in a change in signal.[4] By default, the nature of the linker and the surface density of the redox-labeled polymer chains play a pivotal role in the optimization of the sensitivity of such a sensor. Long linear molecular chains such as synthetic polymers[5] and DNA strands end-capped with an electrochemically active label[6] have been shown to give faradaic currents

T. Steentjes, Prof. P. Jonkheijm, Prof. J. Huskens
Molecular NanoFabrication
MESA + Institute for Nanotechnology
University of Twente
P.O. Box 217, 7500AE Enschede, The Netherlands
E-mail: j.huskens@utwente.nl

Dr. S. Sarkar, Prof. S. G. Lemay
NanoIonics
MESA + Institute for Nanotechnology
University of Twente
P.O. Box 217, 7500AE Enschede, The Netherlands
E-mail: s.g.lemay@utwente.nl

DOI: 10.1002/smll.201603268

dictated by the diffusional motion of the redox moiety. This is in contrast with surface-immobilized systems in which the redox center is located at a fixed distance from the surface and the electron transfer rate depends exponentially on the distance to the surface.[7]

A further increase in sensitivity can be achieved by the use of electrochemical mediators that replenish the oxidized surface layer.[8] Re-activation of the diffusing species in the presence of a second electrode providing an opposing reducing or oxidizing potential, as is performed in scanning electrochemical microscopy (SECM) and in nanofluidic devices,[9] provides a significant amplification of the faradaic current due to redox cycling. This concept has been exploited for biodetection with increased sensitivity.[10] Alternatively, if the second electrode is sufficiently close to the surface to get in contact with the electrochemically active layer, the electrode can take the role of the mediator by replenishing the oxidized/reduced species directly. Such a strategy has been employed using a conductive atomic force microscopy tip positioned on top of poly(ethylene glycol) (PEG)[11] and DNA[12] layers, which allows the direct measurement of the redox cycling current provided by the bounded diffusion of the electrode-attached redox labels.

Nanodevices with nanometric electrode spacings, comparable to the molecular lengths of the surface-attached polymer chains, provide an excellent basis for electrochemical devices in which electron shuttling can occur in the absence of a mediator. This approach further promises the well-controlled and reproducible architecture of a closed solid-state device as well as integration with microfluidics, sample handling, and signal processing.[13] Several device architectures have been demonstrated that lend themselves to miniaturization down to the nanometer scale, including interdigitated electrode arrays,[14] recessed ring electrodes,[15] and thin-layer cells.[9,16] As of yet, however, no such system has been reported in a device configuration where surface-attached redox couples are directly replenished due to the effect of the second electrode without the need of a mediator.

Herein we report nanofluidic devices with two opposing microscale electrodes spaced by a sub-100 nm gap and their functionalization with electrochemically active end-capped polymers in order to study their ability to transfer electrons between the electrodes across the nanogap in the absence of a mediator. We compare the effects of different polymer length and length distribution, as well as the effect of changes in surface density, on the measured current.

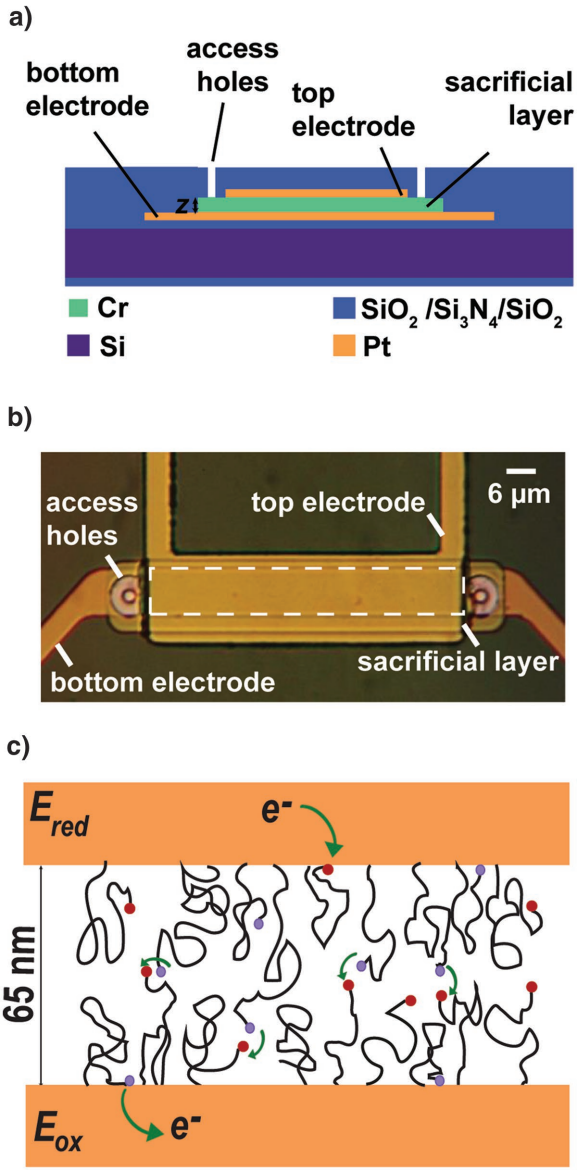

Figure 1. a) Schematic diagram of the cross-section of the nanodevice prior to sacrificial layer etching (not drawn to scale), where z = 65 nm represents the height of the nanogap. b) Optical microscopy image of the top view of a Type II device before the sacrificial layer was etched. The dotted white rectangle represents the active area. c) The nanogap electrodes were functionalized with ferrocene end-capped PEG chains. The PEG layers at opposing electrodes are expected to interpenetrate to allow a current to flow from the reducing to the oxidizing electrode by a sequence of electrode–Fc, Fc–Fc, and Fc–electrode electron transfer steps. Reduced ferrocene groups are depicted in purple, oxidized ferrocenium cation moieties in red, and electron transfer steps in green.

2. Results and Discussion

The nanogap devices used here (**Figure 1**a) consist of two planar rectangular platinum electrodes that are separated by a distance of 65 nm. To fabricate the nanofluidic channel, a sacrificial chromium layer was sandwiched between two platinum electrodes followed by wet etching of the chromium to open up the nanochannel. Two access holes acted as the inlets to the nanochannel. The active region for redox cycling is defined by the overlapping area of the two electrodes, as indicated in Figure 1b. Two different types of nanofluidic devices were used (Type I and Type II), the devices differing primarily in the dimensions of the active region (30 µm^2 for Type I and 300 µm^2 for Type II). A larger active region is expected to trap a likewise larger number of redox molecules between the electrodes, leading to a linear scaling of the current with the area of the active region. This was confirmed here experimentally, as described further below.

The platinum electrodes were modified with cystamine, resulting in a monolayer with exposed amine groups. Onto

this monolayer, bifunctional PEG chains were grafted via a reactive succinimide group present on one end of the chain. The other end bore a redox-active ferrocene (Fc) label that was used for electrochemical detection. Three lengths of PEG, "long" (PEG_{10k}; M_n = 10 ± 2.8 kDa; single standard deviation, polydispersity index PDI = 1.08; average, fully extended chain length L of 79 nm), "intermediate" (PEG_{5k}; M_n = 5.0 ± 1.4 kDa, equal PDI; L = 40 nm), and "short" (PEG_{3k}; M_n = 3.4 ± 0.96 kDa, equal PDI; L = 27 nm), were used in this study to probe the possible effects of chain length and surface density on the current. The PDI causes the polymers to have a rather broad length distribution as schematically shown in Figure S1 (Supporting Information). Electron transfer is expected to occur from the reducing electrode onto an oxidized Fc (ferrocenium) group that, upon diffusion, can transfer the electron to another Fc group of another PEG chain. Because the polymer lengths used here allow interpenetration of the chains immobilized at the opposing electrodes, the Fc–Fc electron transfer may occur from a moiety attached to the reducing electrode onto the one that is immobilized at the oxidizing electrode. Finally, diffusion of a reduced Fc to the oxidizing electrode allows the transfer of the electron between them. These electron transfer steps are schematically shown in Figure 1c. Differences in polymer length and their coverage on the electrodes are expected to influence the surface density of polymer and Fc moieties, the degree of interpenetration of the opposing immobilized layers in the nanogap device, and possibly the diffusion rate of the Fc moieties within the polymer layer. These aspects all contribute to the frequencies of electrode–Fc and Fc–Fc electron transfer events that together define the current.

The nanogap electrodes were initially functionalized with PEG for at least 3 h in order to obtain maximum surface densities. To make sure that all physisorbed PEG molecules were removed from the electrodes, the device was held in a beaker with Milli-Q water and vigorously stirred for at least 10 min. Without this procedure, the redox signal decreased during flow, while the rinsing procedure resulted in signals that were stable for the duration of the experiments. Additionally, control experiments, using mercaptoethanol instead of cystamine thus prohibiting the attachment of the Fc-modified PEG, showed complete removal of redox activity upon applying the same rinsing method (see Figure S2, Supporting Information), and thus confirmed the suitability of this method.

In order to measure the surface densities at the electrodes, the top and bottom electrodes were connected and cycled as one electrode as shown in **Figure 2**a.[17] The results are illustrated in Figure 2b, which shows a cyclic voltammogram measured on a Type I device grafted with PEG_{10k}. The recorded voltammogram is characteristic for surface-attached species, with a peak separation of less than 59 mV for all scan rates employed, a formal potential (E_0') of 0.3 V versus Ag/AgCl, and a peak current (I_p) that increases linearly with the scan rate (Figure 2c).[18] For surface-attached species, the charge under the peak is proportional to the total number of electrons transferred and can be used to calculate the surface density Γ using $\Gamma = Q/nF(A_{top} + A_{bottom})$. Here Q is the measured charge (as shown in Figure 2b), n is the number of electrons transferred per ferrocene moiety (n = 1), F is the Faraday constant, and A_{top} and A_{bottom} are the geometric surface areas of the two electrodes exposed to the solution. A surface density of 19 pmol cm^{-2} was calculated in this case, corresponding to an average spacing of 3 nm between the polymer chains. The latter value is smaller than the calculated Flory radius (R_f = 9.1 nm) of the polymer coils; the value of R_f for good solvents can be calculated from $R_f = aN^{3/5}$, where a = 0.35 nm is the monomer length[19] and N = 227 is the degree of polymerization. Therefore it can be concluded that the polymer was attached to the surface in a loose brush conformation, extending upward from the electrode surface.[11,20]

Subsequently, the two electrodes were addressed separately: a reducing potential (0 V) was applied to the bottom electrode, while the potential of the top electrode was cycled between 0 and 0.6 V (**Figure 3**a). When the potential of the sweeping electrode passed E_0', oxidized ferrocenium species attached to the PEG molecules could regain an electron, either by diffusion to the reducing electrode or by electron transfer from a Fc group attached to this electrode; the opposite being true for reduced species contacting the oxidizing electrode. Combined with Fc–Fc electron transfer between moieties attached to opposite electrodes caused by layer interpenetration (Figure 1c), these electron transfer events gave rise to a redox cycling current. The redox cycling currents measured at the two electrodes are expected to

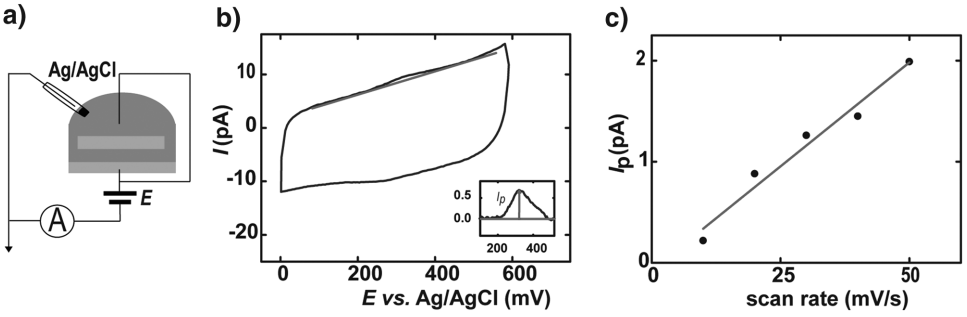

Figure 2. a) Schematic diagram of the measurement configuration when both electrodes are cycled together as one electrode. b) Cyclic voltammogram of ferrocene end-capped PEG_{10k} functionalized electrodes measured in a Type I device at both electrodes simultaneously in a 1 m $NaClO_4$ solution (scan rate 20 mV s^{-1}). The inset shows the baseline-corrected anodic peak, the area of which was integrated to extract the surface charge Q and the corresponding surface density (Γ = 19 pmol cm^{-2} in this case). c) Plot of the peak current versus scan rate, indicating a linear increase of the peak current with the scan rate.

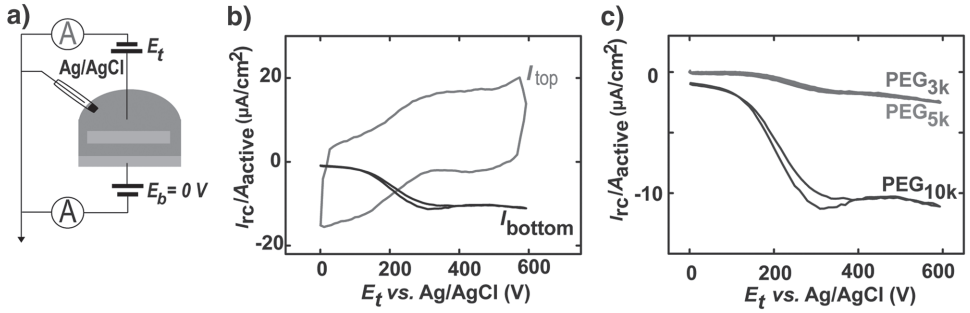

Figure 3. a) Schematic diagram of the measurement configuration showing that the top electrode is cycled (red) while the bottom electrode is fixed at 0 V (black). b) Simultaneously recorded voltammograms for PEG_{10k} (Type II device; $\Gamma = 8.8$ pmol cm^{-2}). c) Comparison of the redox cycling current obtained from PEG_{10k} (data from panel (b)), PEG_{5k} (Type I device; $\Gamma = 25$ pmol cm^{-2}), and PEG_{3k} (Type II device; $\Gamma = 70$ pmol cm^{-2}). All measurements were performed at a scan rate of 50 mV s^{-1} and the currents were normalized by the area A_{active} to facilitate comparison.

have the same magnitude but opposite signs. The resulting cyclic voltammograms for PEG_{10k}, measured on a Type II device with a surface density of 8.8 pmol cm^{-2}, are shown in Figure 3b, where the simultaneously measured currents through each of the two working electrodes are plotted. The current at the electrode being cycled includes a large capacitive contribution which is marked by a pronounced hysteresis (Figure 3b, red curve). This capacitance results in part from the electrical double layer in regions where the electrode is exposed to the solution as well as from the capacitance of the connecting wires, which have a relatively large area and are only protected from the solution by a thin passivating layer of $SiN/SiO_2/SiN$. For this reason we concentrate our analysis below on the current measured at the electrode held at a fixed potential, which nicely isolates the redox cycling component.

Additionally, in order to probe the effect of PEG length, a Type I device was functionalized with PEG_{5k} and a Type II device with a tenfold larger active area was used for PEG_{3k}. Figure 3c shows the obtained redox cycling currents normalized to the area of the active region, A_{active}, for the three different devices. The steady state redox cycling current obtained for PEG_{10k} is nearly an order of magnitude higher than that obtained for PEG_{5k}. This is attributed to the PEG_{5k} layers at the opposing electrodes experiencing less layer interpenetration and thus a less frequent Fc–Fc electron transfer between Fc-PEGs immobilized at opposite electrodes. Only the ferrocene on the sweeping electrode is expected to oxidize, but since the ferrocene moieties on both electrodes can extend half-way through the nanogap, the ferrocenes attached to the opposing reducing electrode can donate electrons and act as a mediator. Since the amount of ferrocene moieties attached to the electrodes is known ($\Gamma = 25$ pmol cm^{-2} in this case), a concentration of 7.4×10^{-3} M ferrocene can be calculated to be present inside the active region. This is a concentration comparable to mediators used in SECM for measurements on monolayers.[21] PEG_{3k} is even shorter and was not expected to be able to exchange electrons as the average, fully extended length, $L = 27$ nm, does not allow the ferrocene labels attached to the electrode to reach half-way across the channel. However, at the present PDI of 1.08, corresponding to a standard deviation of 0.96 kDa (or a total of 4.4 kDa) the length of a significant fraction of the polymer chains can extend beyond 34 nm, which exceeds half the gap separation. This makes it plausible that also in this case a fraction of polymer chains is capable of participating in electron transfer. Combined with the higher coverage for PEG_{3k} (70 pmol cm^{-2}), this explains the observed similar current values obtained for PEG_{5k} and PEG_{3k}.

The experiments of Figures 2 and 3 were repeated in several additional devices for all three chain lengths, and the results are summarized in **Figure 4**. The measured surface densities decreased with increasing polymer length (Figure 4a), as expected since the increased Flory radius leads to steric hindrance. Some scatter is observed in the data, which we attribute primarily to surface roughness: the area values are based on the geometric surface area and averaged over both electrodes, whereas the surface roughness is not the same for both electrodes (see Figure S3, Supporting Information) and can vary between devices. The corresponding redox cycling currents were recorded simultaneously and were similar to the examples shown in Figure 3. To get a clear picture of the effect of the linker length, the redox cycling currents were normalized to the surface density according to $v = Irc/(eN_{active})$ (with e being the charge of an electron and N_{active} the amount of PEG-Fc molecules in the active area)—yielding the rate of electron transfer per available ferrocene group—as presented in Figure 4b (real currents are reported in Figure S4, Supporting Information). This analysis shows that a single PEG_{10k} chain functionalized with a ferrocene end group is able to transfer on average six electrons to the opposing electrode per second, whereas the

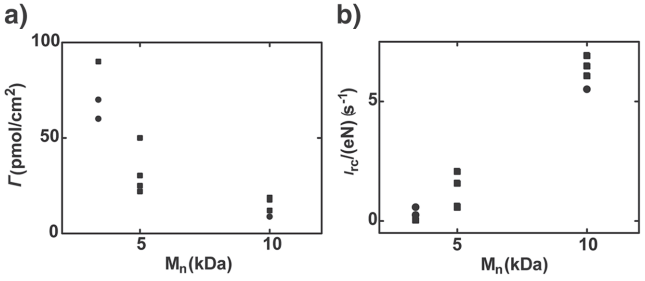

Figure 4. a) The effect of linker length on the obtained maximum surface density after 3 h functionalization, and b) the corresponding redox cycling currents, presented as the rate of electrons transferred per PEG chain. The measurements were performed on both types of devices, Type I = ■, Type II = ●.

electron transfer rate drops to 1 s^{-1} per ferrocene for PEG_{5k}, reflecting the decrease in polymer length and the lower frequency of Fc–Fc electron transfer events between oppositely immobilized chains. It also becomes clear that although the measured redox cycling currents for PEG_{3k} are not significantly lower than for PEG_{5k}, the rate of electrons transferred per ferrocene available is only 0.3 s^{-1} for PEG_{3k}, and thus the measured redox cycling currents for PEG_{3k} compared to PEG_{5k} are the result of a higher surface density while a smaller fraction of the polymer chains is long enough to contribute to electron transfer.

When considering the mechanism by which the electrons are transferred, it was anticipated that the polymer length of PEG_{10k} is long enough to enable the attached ferrocene moiety to travel to the opposing electrode, whereas the chain length for PEG_{5k} can only provide for electron transfer between the ferrocene moieties itself inside the channel in the zone where layer interpenetration and Fc–Fc electron transfer events between oppositely immobilized chains occur. Not taking into account the dispersity of the polymers, the length of 40 nm of PEG_{5k} gives rise to a 15 nm exchange zone inside the 65 nm channel where the polymer chains from both electrodes can overlap and the ferrocene moieties can exchange electrons. For the PEG_{10k} chains to reach the opposing electrodes they have to stretch outward and penetrate through the polymer layer resulting in an exchange zone of 65 nm (the entire channel). Next to larger exchange zone by a factor of four, the concentration of ferrocene inside the channel is on average a factor of two lower for PEG_{10k} than for PEG_{5k} due to the lower surface densities, which corresponds to an overall expected higher activity of a factor of two for PEG_{10k}. Additionally, for PEG_{10k} there is no need to stretch fully to reach an opposing PEG chain. Taking all these factors into account, we attribute the observed fivefold higher activity of PEG_{10k} compared to PEG_{5k} to electron transfer dominated by exchange between the diffusing and interpenetrating ferrocene moieties in both cases, rather than direct transfer to the opposing electrode. We expect the same mechanism to hold for PEG_{3k} as well, when taking the dispersity into account. In this case, only a fraction of the molecules is sufficiently long to allow some interpenetration of the chain ends from opposing electrodes which, combined with the higher surface density, leads to the observed three times lower activity compared to PEG_{5k}. When taking the polymer chain length dispersities into account for all polymers, the interpenetration and exchange zones do not have sharply defined boundaries, but the exchange extends outside of the given borders with decreasing probabilities. Since proper electron transfer rate calculations would have to take into account the polymer length distributions, probability distributions of the distance between the Fc end group and the electrode, collision frequencies, polymer surface densities, diffusion rates, and Fc–Fc and Fc–electrode electron transfer rates, we did not attempt this here. From the almost linear behavior observed for the electron transfer per Fc moiety for the polymers studied here (Figure 4b) and the arguments given above, we conclude that the interpenetration and Fc–Fc exchange model (as depicted in Figure 1c) holds for all polymer lengths studied here.

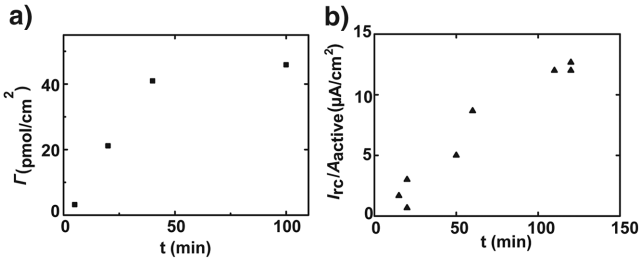

Figure 5. a) Surface densities on macroelectrodes and b) redox cycling currents in nanogap devices for PEG_{10k} as a function of the incubation time.

The conformation of polymers grafted to the surface depends on the surface density, with the polymers existing in a mushroom conformation at low surface densities, where the polymers are isolated from their neighboring chains, and becoming more brush-like with increasing surface density as the surface concentration passes a critical surface density.[20] In order to study a possible effect of the PEG density and conformation regime on the redox cycling currents, Type I devices were functionalized with different surface densities of PEG_{10k}, by changing the time the molecules were allowed to react with the cystamine monolayer. The resulting redox cycling currents were plotted versus the incubation time, as shown in **Figure 5**. The surface densities, especially for short reaction times, were too low to give clearly distinguishable peaks in the cyclic voltammograms, and no reliable surface densities could be recorded. Therefore the redox cycling currents were compared with surface densities determined from experiments on macroelectrodes. As can be seen in Figure 5a, the obtained surface densities on the macroelectrodes reach a plateau around 40 pmol cm^{-2}, which is more than a factor of two higher than the values obtained inside the nanogap devices (Figure 4a). Therefore it is expected that the surface densities inside the nanogap devices are still in the linear regime (left side of Figure 5a) for all incubation times used, probably due to slower mass transport compared to the macroelectrodes. Indeed, it can be seen (Figure 5b) that the recorded redox cycling currents increase linearly with the incubation time. It can thus be concluded that the increase in current with increasing reaction times is mostly the result of the increase of ferrocene density and not of a change in polymer conformation. Due to the bulky nature of the PEG_{10k} molecule, all used reaction times result in polymers present in a loose brush conformation (the maximum surface density for the mushroom configuration for PEG_{10k} is calculated as 2 pmol cm^{-2}),[20] and no dramatic change of behavior could be observed.

3. Conclusion

We have shown that surface-tethered PEG polymer chains with redox-active end groups allow the transfer of electrons between the electrodes in nanogap devices in the absence of an electrochemical mediator. The primary condition that needs to be met is that the polymer chains of the opposing electrodes can interpenetrate so that oxidized and reduced

ferrocene moieties can exchange electrons. The activity per Fc unit, as defined by the average number of electrons transferred per Fc moiety, is strongly dependent on the chain length, but not on the chain density in the loose brush density range studied here. The chain length effect is interpreted primarily by the increasing thickness of the channel zone in which exchange can occur and the increasing fraction of the polymers that can reach this exchange zone. The overall measured cycling currents are additionally dependent on the surface density, which is lower for longer polymers and thus counteracts to some extent the enhanced activities observed for the longer PEGs. All polymer lengths studied here were found to obey this same interpenetration and electron exchange model.

The findings of this study can contribute to an enhanced understanding and improved performance of biosensing devices that use redox cycling in surface-tethered receptor devices as the main amplification mechanism, such as in DNA hairpin-like detection schemes. For example, if a probe DNA molecule that allows hairpin formation is inserted in an immobilized polymer chain, binding of a complementary target DNA can break up the hairpin leading to an apparent lengthening of the polymer chain and thus to an increased layer penetration and enhanced current. A single binding event thus affects the electron transfer of many electrons, hence causing amplification. An increase in current, and with that an increase in sensitivity, can be expected if the height of the nanochannel is more finely tuned toward the length of the linker. At the same time, the selectivity between bound and unbound receptors can be improved when the polymer length distribution is more narrow and when the extended chain length is close to half of the channel width, so that small changes in polymer stiffness and length have large effects on the probabilities of chain interpenetration and electron exchange.

4. Experimental Section

Materials: Reagents and solvents were purchased from Sigma-Aldrich; high-purity water (Milli-Q) was used (Millipore, R = 18.2 MΩ). All bis-NHS-functionalized PEGs were purchased from Nanocs and had a reported dispersity of 1.08.

Device Fabrication: A 4 in. Si wafer was isolated with 500 nm thick thermally grown SiO_2. A Pt bottom electrode, a Cr sacrificial layer and a Pt top electrode were then consecutively deposited by electron-beam evaporation of 20, 60, and 100 nm of metal, respectively, and patterned using a lift-off process based on a positive photoresist (OIR 907-17, Arch Chemicals). Thereafter, a passivation layer consisting of 90 nm/325 nm/90 nm thick PECVD SiO_2/Si_3N_4/SiO_2 was deposited. Access holes were then etched through the passivation layer in by reactive ion etching, reaching the Cr sacrificial layer. Lastly, the sacrificial layer was etched by placing a drop of chromium etchant (BASF, Chromium Etch Selectipur) at the inlets of the nanochannel. Additional details of the fabrication process have been described elsewhere.[22]

Electrochemical Experiments in the Nanodevice: The electrodes were cleaned prior to the measurements by cycling their potential in 0.5 M H_2SO_4 between –0.15 and 1.2 V at 50 mV s^{-1} until a stable voltammogram was obtained. The devices were rinsed with Milli-Q water and a polydimethylsiloxane (PDMS) reservoir was positioned above the device, which was filled with a 2×10^{-3} M solution of cystamine and left overnight. Subsequently, the devices were rinsed with a copious amount of water and filled with a 0.2×10^{-3} M Fc-PEG-NHS solution in water for 3 h or the incubation times indicated in Figure 5, after which the device was immersed in a beaker with Milli-Q water, which was vigorously stirred for at least 5 min (control measurements have shown that this is sufficient time to remove all physisorbed PEG chains from the channel; see Figure S2, Supporting Information). Before measurements, the devices were filled with a 1 M $NaClO_4$ supporting electrolyte solution, and a standard Ag/AgCl electrode (BASi, MF 2079, RE-5B) inserted in the PDMS reservoir was used as the reference electrode. No counter electrode was used as the current through the reference is minimal in this configuration. Two transimpedance amplifiers (Femto, DDPCA-300) were used to apply potentials to the two working electrodes with respect to the reference electrode and monitor the currents through these electrodes.

Supporting Information

Supporting Information is available from the Wiley Online Library or from the author.

Acknowledgements

T.S. and S.S. contributed equally to this work. The authors gratefully acknowledge financial support from the European Research Council (ERC; eLab4Life and ECnano projects) and The Netherlands Organization for Scientific Research (NWO; Vici 700.58.443). This publication was further made possible by Grant number 1R01HG006882-01 from National Institutes of Health (NIH); its contents are solely the responsibility of the authors and do not necessarily represent the official views of NIH.

[1] M. A. Hamburg, F. S. Collins, *N. Engl. J. Med.* **2010**, *363*, 301.
[2] J. Wang, *Biosens. Bioelectron.* **2006**, *21*, 1887.
[3] a) J. Kirsch, C. Siltanen, Q. Zhou, A. Revzin, A. Simonian, *Chem. Soc. Rev.* **2013**, *42*, 8733; b) V. Perumal, U. Hashim, *J. Appl. Biomed.* **2014**, *12*, 1; c) D. G. Rackus, M. H. Shamsi, A. R. Wheeler, *Chem. Soc. Rev.* **2015**, *44*, 5320.
[4] a) C. Fan, K. W. Plaxco, A. J. Heeger, *Proc. Natl. Acad. Sci. USA* **2003**, *100*, 9134; b) Y. Xiao, X. Qu, K. W. Plaxco, A. J. Heeger, *J. Am. Chem. Soc.* **2007**, *129*, 11896; c) Y. Xiao, X. Lou, T. Uzawa, K. J. I. Plakos, K. W. Plaxco, H. T. Soh, *J. Am. Chem. Soc.* **2009**, *131*, 15311.
[5] a) A. Anne, C. Demaille, J. Moiroux, *Macromolecules* **2002**, *35*, 5578; b) A. Anne, J. Moiroux, *Macromolecules* **1999**, *32*, 5829; c) D. N. Blauch, J. M. Saveant, *J. Am. Chem. Soc.* **1992**, *114*, 3323.
[6] a) A. Anne, A. Bouchardon, J. Moiroux, *J. Am. Chem. Soc.* **2003**, *125*, 1112; b) K. C. Huang, R. J. White, *J. Am. Chem. Soc.* **2013**, *135*, 12808; c) N. Hüsken, M. Gębala, F. La Mantia, W. Schuhmann, N. Metzler-Nolte, *Chem. Eur. J.* **2011**, *17*, 9678.

[7] a) J. F. Smalley, S. W. Feldberg, C. E. D. Chidsey, M. R. Linford, M. D. Newton, Y.-P. Liu, *J. Phys. Chem.* **1995**, *99*, 13141; b) K. Weber, L. Hockett, S. Creager, *J. Phys. Chem. B* **1997**, *101*, 8286; c) H. O. Finklea, D. D. Hanshew, *J. Am. Chem. Soc.* **1992**, *114*, 3173.
[8] S. A. Merchant, M. T. Meredith, T. O. Tran, D. B. Brunski, M. B. Johnson, D. T. Glatzhofer, D. W. Schmidtke, *J. Phys. Chem. C* **2010**, *114*, 11627.
[9] M. A. G. Zevenbergen, D. Krapf, M. R. Zuiddam, S. G. Lemay, *Nano Lett.* **2007**, *7*, 384.
[10] a) C. Zhao, G. Wittstock, *Angew. Chem. Int. Ed.* **2004**, *43*, 4170; b) L. Rassaei, K. Mathwig, S. Kang, H. A. Heering, S. G. Lemay, *ACS Nano* **2014**, *8*, 8278.
[11] J. Abbou, A. Anne, C. Demaille, *J. Am. Chem. Soc.* **2004**, *126*, 10095.
[12] K. Wang, C. Goyer, A. Anne, C. Demaille, *J. Phys. Chem. B* **2007**, *111*, 6051.
[13] L. Rassaei, P. S. Singh, S. G. Lemay, *Anal. Chem.* **2011**, *83*, 3974.
[14] a) V. A. T. Dam, W. Olthuis, A. van den Berg, *Analyst* **2007**, *132*, 365; b) E. D. Goluch, B. Wolfrum, P. S. Singh, M. A. G. Zevenbergen, S. G. Lemay, *Anal. Bioanal. Chem.* **2009**, *394*, 447; c) A. K. Samarao, M. J. Rust, C. H. Ahn, *Proc. IEEE Sens.* **2007**, 644.
[15] C. Ma, N. M. Contento, L. R. Gibson, P. W. Bohn, *ACS Nano* **2013**, *7*, 5483.
[16] a) E. Kätelhön, B. Hofmann, S. G. Lemay, M. A. G. Zevenbergen, A. Offenhäusser, B. Wolfrum, *Anal. Chem.* **2010**, *82*, 8502; b) J. Xiong, Q. Chen, M. A. Edwards, H. S. White, *ACS Nano* **2015**, *9*, 8520.
[17] For the determination of the surface densities, the electrodes could not be cycled individually as the two electrodes are capacitavely coupled, giving rise to a situation analogous to the positive-feedback mode of SECM with an unbiased electrode. See: A. I. Oleinick, D. Battistel, S. Daniele, I. Svir, C. Amatore, *Anal. Chem.* **2011**, *83*, 4887.
[18] A. J. Bard, L. R. Faulkner, *Electrochemical Methods: Fundamentals and Applications*, 2nd ed., John Wiley & Sons, New York **2001**.
[19] C. Allen, N. Dos Santos, R. Gallagher, G. N. C. Chiu, Y. Shu, W. M. Li, S. A. Johnstone, A. S. Janoff, L. D. Mayer, M. S. Webb, M. B. Bally, *Biosci. Rep.* **2002**, *22*, 225.
[20] P. G. De Gennes, *Macromolecules* **1980**, *13*, 1069.
[21] B. Liu, A. J. Bard, M. V. Mirkin, S. E. Creager, *J. Am. Chem. Soc.* **2004**, *126*, 1485.
[22] a) M. A. G. Zevenbergen, B. L. Wolfrum, E. D. Goluch, P. S. Singh, S. G. Lemay, *J. Am. Chem. Soc.* **2009**, *131*, 11471; b) S. Kang, K. Mathwig, S. G. Lemay, *Lab Chip* **2012**, *12*, 1262.

Received: September 28, 2016
Revised: November 11, 2016
Published online: December 16, 2016

